Re-equilibration of glass and CO2 inclusions in xenolith olivine: A TEM study

Article *in* American Mineralogist · October 2000

DOI: 10.2138/am-2000-1007

CITATIONS
41

READS
86

2 authors:

Cecilia Viti
Università degli Studi di Siena
102 PUBLICATIONS **3,036** CITATIONS
SEE PROFILE

Maria Luce Frezzotti
Università degli Studi di Milano-Bicocca
137 PUBLICATIONS **3,635** CITATIONS
SEE PROFILE

American Mineralogist, Volume 85, pages 1390–1396, 2000

Re-equilibration of glass and CO_2 inclusions in xenolith olivine: A TEM study

CECILIA VITI AND MARIA-LUCE FREZZOTTI*

Dipartimento Scienze della Terra, Università di Siena, Via Laterina 8-53100 Siena, Italy

ABSTRACT

CO_2-rich fluid inclusions were observed in olivine from mantle xenoliths from the Island of Tenerife, Canary Islands. Inclusions that are present in deformed olivine porphyroclasts consist of CO_2 fluids + minor high-alkali, silica-rich glass ± Ni-Fe sulfides. Homogenization temperature distributions reveal that most of the inclusions (originally trapped at mantle conditions) re-equilibrated to lower density values.

Transmission electron microscope (TEM) studies indicate that most fluid inclusions appear as perfectly euhedral negative crystals, with variable shape (from prismatic to equant), size (from <0.02 to 0.15 μm), and inner texture. Different kinds of negative crystals may coexist in the same trail of inclusions. Inclusions are commonly connected to structural defects (dislocation arrays formed after fracture healing), which represent a possible path for leakage of the fluid phase. These microstructures, undetectable by optical microscopy, could have modified the original composition and/or density of the inclusions through CO_2 diffusion; consequently, they should be taken into account for the correct interpretation of microthermometric results.

INTRODUCTION

Fluid inclusions are common tools for reconstructing the *P-T-X* history of mineral growth and subsequent evolution. Consequently, the conclusions we can derive from inclusion studies are of great interest for the understanding of different petrological and geological processes. The use of fluid inclusions to infer pressure and temperature data is based on the hypothesis that inclusions are closed systems, that is, they never changed their volume (isochoric), molar volume (volume/number of moles), and chemical composition after trapping in the host mineral.

Recent studies, however, have shown that fluid inclusions might be affected by reactions, deformation, and leakage with a change in density and/or composition (i.e., a re-equilibration process; Touret 1992; Vytik and Bodnar 1995a, 1995b and references therein). Although most studies concentrate on H_2O-rich inclusions in quartz, re-equilibration also affects CO_2 inclusions in olivine crystals, particularly those originating at mantle depths (e.g., Wanamaker and Evans 1989): only a few inclusions can be considered representative of the original trapping conditions in the upper mantle (e.g., Frezzotti et al. 1992; Neumann et al. 1995; Szabo and Bodnar 1996). Ultramafic xenoliths (including those from the Canary Islands) are generally interpreted as pieces of refractory mantle that were incorporated in the fast-ascending (0.1–5 m/s, Spera 1984) alkali-basalt magma. Because of the rapid drop of external pressure occurring at very high temperatures (1100–1200 °C), fluid pressure exceeds the confining pressure and inclusions may decrepitate ($P_{\text{fluid inclusion}} > P_{\text{lith}}$). Re-equilibration by partial decrepitation resets the fluid inclusion density to lower values: these lower values are given petrogenetic significance because they are considered representative of the pressure conditions of shallow magma chamber residence, allowing one to constrain the depths of magma accumulation (Frezzotti et al. 1991; Szabo and Bodnar 1996; Hansteen et al. 1998).

Non-decrepitative leakage of fluid inclusions may occur by diffusion of molecules from the inclusions into the host mineral. Usually the transport mechanism is not "lattice" diffusion, and it strongly depends on the presence of "open spaces" in the crystal structure, along which diffusion can occur at higher rates. These open spaces are represented by crystal defects—as vacancies, dislocations, stacking faults, intergrowth defects, and other structural misfits (e.g., Veblen 1985). Pipe diffusion along dislocation cores is an example of enhanced diffusion by crystal defects.

The occurrence of these "open channels," connected to re-equilibrated fluid inclusions, may not be evident at the optical microscopy scale: in such cases, a TEM investigation is necessary to understand the processes by which the fluid leakage takes place. An exhaustive TEM study on fluid inclusion re-equilibration was performed by Bakker and Jansen (1994). These authors showed a preferential leakage of H_2O with respect to CO_2 in synthetic H_2O-CO_2 fluid inclusions through dislocations that were formed by fluid overpressure in the inclusion. Preferential loss of H_2O is explained as due to its chemical-physical affinity with the host quartz and to the lower size of the H_2O molecules with respect to CO_2 molecules (which can further react with H_2O to form larger H_2CO_3 molecules).

The present study deals with CO_2 + glass inclusions in olivine grains from mantle xenoliths. Microthermometric measurements revealed that most inclusions were re-equilibrated at lower densities, with a wide spread in the measured density data. Because no evidence of decrepitation was observed at

* E-mail: frezzottiml@unisi.it

0003-004X/00/0010–1390$05.00

the resolution of the optical microscope, we investigated the same olivine crystals with a TEM to understand the re-equilibration mechanism.

Specimen selection and fluid-inclusion data

Petrography

Ultramafic and gabbroic xenoliths commonly occur in basaltic rocks from the Canary Islands. They contain abundant fluid (CO_2) ± glass inclusions, which are similar on a regional scale. Previous fluid inclusion studies indicate that the xenoliths originated in the mantle at great depth (6–12 kbar pressure), possibly followed by re-equilibration at shallow depth (2–4 kbar pressure) (Hansteen et al. 1991; Siena et al. 1991; Frezzotti et al. 1994; Neumann et al. 1995; Gurenko et al. 1996).

Two xenoliths from Tenerife (TF14-2 and TF 14-48) were selected for a detailed study on the basis of the textural and microthermometric characteristics of the fluid inclusions. The samples are spinel harzburgite consisting of 88–85% modal olivine, 10–15% modal orthopyroxene, and traces of modal spinel (up to 1–2%). Both samples have protogranular to porphyroclastic textures and show evidence for deformation (strained olivine and orthopyroxene porphyroclasts). Similar to the spinel harzburgite suite from other Canary Islands (Neumann 1991), two generations of olivine are present. The first generation consists of large (up to 2 mm), strained and kinked olivine grains that commonly show undulatory extinction (Type I), and the second consists of small (up to 0.5 mm), strain-free polygonal to anhedral olivine grains (Type II). Forsterite contents in both porphyroclasts and neoblasts are similar (between 90 and 92%).

CO_2-rich fluid inclusions are texturally early and are present only in strained porphyroclasts of olivine (Type I) along short, healed intragranular trails that, in kinked host-olivine grains, typically end within single extinction zones (Fig. 1, left). Undeformed Type 2 olivine is free of inclusions. Inclusion sizes range from <2 to 10 μm. CO_2–rich inclusions have regular shapes, ranging from prismatic to equant (Fig. 1, right). Many CO_2-rich fluid inclusions also contain sulfides and/or colorless glass in variable proportions (from 10 to 40 vol%). This textural character suggests simultaneous trapping of a heterogeneous fluid mixture (immiscible CO_2 fluids and silicate melt).

As a reference, two xenoliths from the nearby island of Hierro (HI-24 and HI-55) were also investigated. Fluid inclusions in the Hierro samples were investigated previously by Hansteen et al. (1991). In olivine porphyroclasts they found texturally early CO_2-rich inclusions with densities from 1.1 to 0.65 g/cm^3, corresponding to a maximum pressure of 12 kbar at 1200 °C. These inclusions represent fluids trapped during the mantle evolution of xenoliths that in part escaped resetting of densities to lower values.

Microthermometry

Inclusions selected for microthermometric study showed no evidence for partial decrepitation, such as microfractures radiating from single inclusions, star-shaped contours, and/or haloes of tiny fluid inclusions surrounding each fluid inclusion. All measurements were performed with a Linkam TH600 heating freezing stage at the Centro Studi per il Quaternario e l' Energia Ambientale (C.S. Qu. E.A.–C.N.R.; National Council for Research) in Rome. Calibration was performed using SYNFLINC synthetic fluid-inclusion temperature standards. In the temperature interval between –90 and +40 °C, accuracy was estimated as ±0.1 °C at the standard reference points, and ±0.2 °C at other temperatures.

All selected inclusions froze to solid CO_2 and vapor when cooled to about –90 °C. On heating, instantaneous melting of solid CO_2 occurred at ≈ –56.6 °C (S+V → L+V), indicating the presence of pure CO_2 fluids (CO_2 triple point = –56.6 °C). The purity of the CO_2 fluids was also confirmed by Raman analyses (using the LabRam instrument, of the Jobin Yvon company) at the Università di Siena. On further heating from this temperature, final homogenization of liquid and vapor into liquid (L+V → L) was recorded below 23 °C. In sample TF14-2, temperatures of homogenization to the liquid (ThL) are recorded up to 17.1 °C, with the majority of measurements at 3 °C (Fig. 2); data between 8 and 17 °C may represent re-equilibrated inclusions. Sample TF 14-48 shows a more scattered distribution, with data clustering between 4 and 22 °C. Inclusion density can be determined on the basis of fluid composition and ThL. Densities of inclusions in sample TF14-48 were calculated between 0.95 to 0.69 g/cm^3: the data distribution sug-

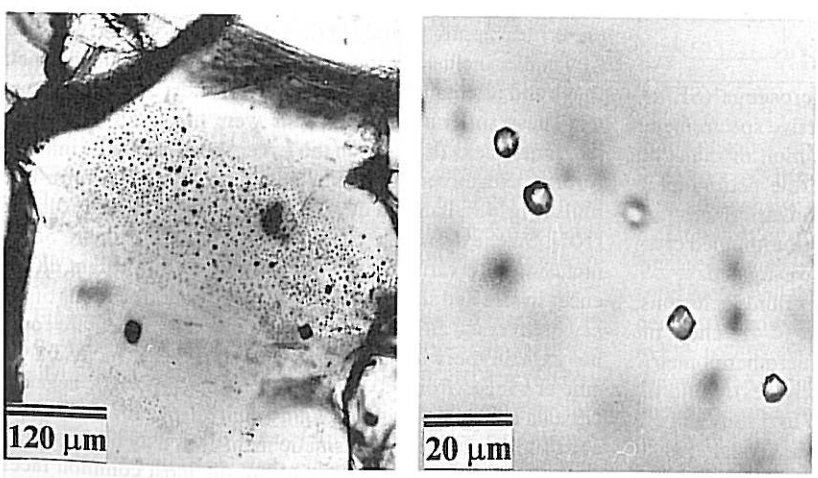

FIGURE 1. (**left**) Intragranular trail of CO_2-rich inclusions typically forming an angle of 60° with respect to the crystal elongation direction. (**right**) Trail of CO_2-rich inclusions with equant negative crystal shape. Note that inclusions are single-phase at room temperature. (Optical microscopy, plane polarized light). Sample TF14-48.

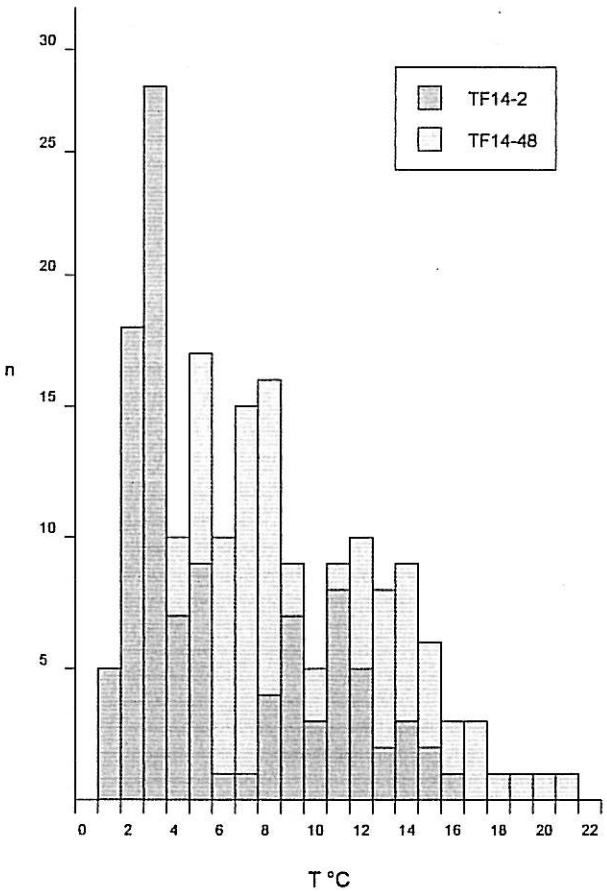

FIGURE 2. Homogenization temperatures of CO_2-rich inclusions in mantle xenoliths from Tenerife (samples TF14-2 and TF14-48). All homogenizations are to the liquid phase (ThL; L+V → L).

gests that the inclusions have lost their original density, although decrepitation was not observed.

Isochores for CO_2 inclusions were calculated using the FLINCOR computer program (Brown 1989) and the equation of state for CO_2 (Kerrick and Jacobs 1981). CO_2 fluids were trapped at mantle depths in the pressure interval of 6–4 kbar (i.e., depths greater than 20 km), assuming a temperature of 1000 °C (local geotherm, Neumann 1991).

SEM observation and EDS data

A Philips XL30 scanning electron microscope (SEM), equipped with an EDAX DX4 energy dispersive spectrometer (EDS), was used to investigate the composition of the solid phases present within the inclusions. Both the petrographic sections (the same as used for microthermometric investigations) and the specimens for the TEM study (ion-thinned crystals glued on copper grids, see later) were investigated.

Olivine crystals contain different kinds of fluid inclusions, which are particularly abundant in sample TF14-48. These inclusions correspond to those selected for microthermometric determinations (early inclusions in type I olivines). Fluid inclusions exhibit variable shape and size (up to 5 μm) and are arranged in wide trails at ~60° with respect to crystal elongation. The compositions of the solid phases occurring within the inclusions have been determined by EDS, even though analytical contamination by the host olivine possibly occurred due to the small size of the inclusions. The bright grains in backscattered electron (BSE) images are iron-nickel sulfides (with Fe/Ni ranging from 0.5 up to 4), whereas the darker material corresponds to a glass. Analyses of this glass reveal high K_2O and Na_2O, contents (overall range in wt%: SiO_2: 46–54; Na_2O: 5–6; K_2O: 1.5–5; Al_2O3: 13–19; MgO: 13–29; FeO 2–6), and they cannot be related to the host alkali basalt. The MgO and SiO_2 contents reflect some analytical contamination by the host olivine. Similar alkali-rich, high-silica melts are commonly observed in $CO_2 \pm$ glass inclusions in mantle xenoliths from the Canary Islands and elsewhere. There is at present quite a lively discussion regarding the role and origin of these alkali-rich melts at mantle conditions, although most authors (cf., Schiano and Clocchiatti 1994; Neumann et al. 1995; Wulff-Pedersen et al. 1996) have agreed upon the major role of such melts as mantle metasomatic agents.

TEM OBSERVATIONS

TEM investigations were performed using a Philips 400T, operating at 120 kV with a nominal point to point resolution close to 4 Å. Two olivine crystals from each xenolith (TF14-48, TF14-2, HI-24, and HI-55) were selected for the TEM study. The crystals were extracted from the same petrographic sections used for fluid-inclusion measurements and then ion-thinned using a Gatan Dual Ion Mill 600. Although different crystal orientations have been investigated, TEM observations have been done mostly in the [001]orientation.

Inclusions and negative crystals

Different kinds of inclusions can be distinguished on the basis of size, shape, and textural arrangement in trails and, despite the different scale, significant similarities can be noticed between trails observed by TEM and SEM. The identification of large inclusions (>1 μm in diameter) is difficult by TEM: they can be distinguished as a quite regular indentation along the thin edge of the sample, owing to a weak tendency to develop negative crystal faces (Fig. 3, left). These inclusions are empty, due to the ion-thinning. Several contrast heterogeneities can appear in the enclosing olivine, in particular, linear contrast features starting from the inclusions and extending up to ~0.7 μm approximately in the [100] direction (Fig. 3, right).

Smaller inclusions appear as negative crystals, that is, their shape and orientation are imposed by the host mineral symmetry. These small negative crystals were produced by healing the same cracks from which the larger fluid inclusions initially formed. Negative-crystal inclusions form wide, swarm-like trails (Fig. 4a), inclined by ~30–40° with respect to the olivine [100]. Size, external shape, and internal microstructure of the inclusions are variable (as sketched in Fig. 4b). Slight differences in size and shape could be due to different sections of the negative crystal along its [001] axis; however, this feature could not explain the wide range of observed shapes. Inclusion diameter ranges from <0.02 up to 0.1 μm. Typically, negative crystals are equant with a roughly equivalent growth of (010) and (100) faces, even if prismatic inclusions may be present as well. Together with (010) and (100), the most common faces

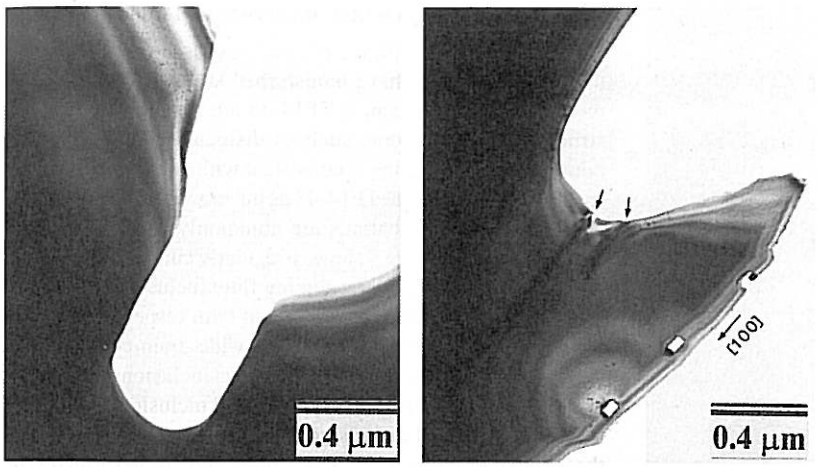

FIGURE 3. TEM images of olivane. (**left**) Regular indentation of the thinning edge, corresponding to a large fluid inclusion. (**right**) Linear contrast features connected to a large inclusion (arrows). A regular trail of smaller prismatic fluid inclusions is also evident, parallel to olivine [100]. Sample TF14-48.

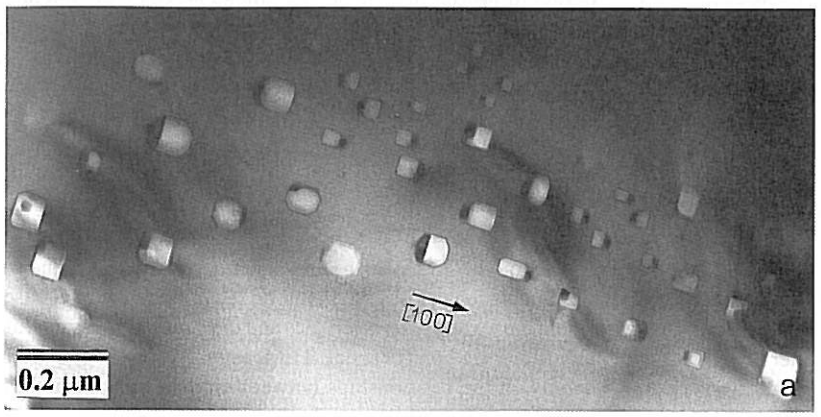

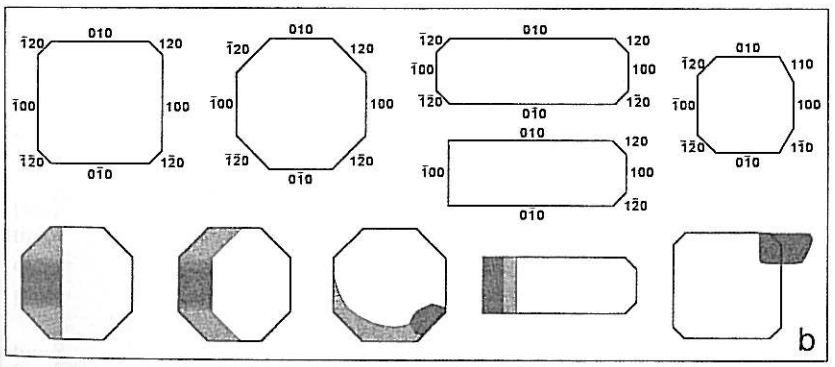

FIGURE 4. (**a**) TEM image of olivine showing negative crystal inclusions in swarm-like trail (the arrow indicates the olivine [100]). Sample TF14-48. (**b**) Common negative crystal habits and inner textural arrangements.

are (120), (110), and (130): the relative growth of each face varies from inclusion to inclusion. Negative crystals may also exhibit an asymmetrical shape [with respect to both (100) and (010) equatorial planes]. The occurrence of the above negative crystals faces agrees well with the "outer" olivine morphology (Fleet 1975; t'Hart 1987a, 1987b).

Figure 5 shows a detail of a prismatic negative crystal, with (010), (100), and (120) faces: the host olivine is imaged as a regular orthogonal array of dots, ~4.7 Å and ~10.3 Å (respectively in the[100] and [010]directions). The ordered structure of olivine ends sharply at the negative crystal faces and no structural defects occur there: such evidence indicates a mature state in the negative crystal evolution.

As regards their inner texture, inclusions in swarm-like trails typically consist of a rounded empty cavity (originally filled by CO_2, lost during ion-thinning) plus a solid phase, which is smeared along (100) or (010) faces. The boundary between the solid phase and the empty space can be parallel to (100), independently from the shape of the negative crystal (inclusion A in Fig. 6, left), or it can be exactly coherent with respect to the shape of the negative crystal (inclusion B in Fig. 6, left). The boundary can also appear as a regular meniscus (inclusions C in Fig. 6, left), indicating that two fluid phases (inferred to be CO_2 fluid and a silicate melt) were present during inclusion trap-

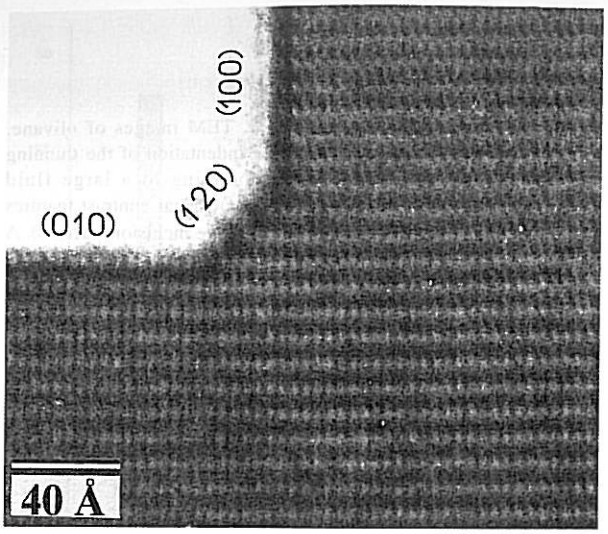

FIGURE 5. High-resolution TEM image of an olivine crystal in the [001] orientation. The (010), (100), and (120) faces of a prismatic negative crystal are evident in the upper left corner. Sample TF14-48.

ping. A dark-faceted grain is commonly observed within the inner solid material (inclusions C in Fig. 6, left), similarly to what is observed with the optical microscope and SEM. The EDS TEM analyses confirm that the dark-faceted grain is an Fe-Ni sulfide. High-resolution images indicate that the Fe-Ni sulfide is present as a crystalline phase. Figure 6 (right) shows the (010) lattice fringes of the host olivine interfering with the lattice fringes of the daughter minerals. The interference between the two sequences of lattice fringes produces a Moiré pattern, whose spacing is ~12 Å.

Relationships between fluid inclusions and microstructures

Except for TF14-48, the olivine crystals (particularly from the Hierro samples) have undisturbed structures. In contrast, olivine grains from sample TF14-48 are affected by different structural perturbations, such as dislocations and subgrain boundaries. This finding is consistent with petrographic observations, which indicate TF14-48 as the most-deformed sample.

Structural perturbations are commonly connected to the fluid inclusions. Figure 7 shows irregularly curved defects, with a typical sigmoidal pattern, linking fluid inclusions in swarm-like trails. These defects are inclined with respect to the general orientation of the trail and show a wide strain-contrast field. Each defect may link two or three distinct inclusions, thus forming a connection between different fluid inclusions.

These structural defects correspond to healing surfaces of the original fractures from which inclusions were formed. The healed fracture is reasonably characterized by a local concentration of crystal defects, as the olivine crystal structure does not fit perfectly at the opposite sides of the fracture. In particular, the geometrical misfit is accommodated by dislocation arrays. Healed surfaces and dislocation arrays, associated with fluid inclusion trails, may represent a favorable path for CO_2 diffusion and may have influenced the fluid-inclusion closed system, by modifying its original composition and density.

DISCUSSION

Although TEM does not represent a routine technique for fluid inclusion studies, it should be recommended in all cases where the textural characteristics and the density data from fluid inclusions are controversial. TEM, in fact, can give important details on the relationships between fluid inclusions and the host mineral, to understand whether inclusions actually behaved as closed systems or if they were re-equilibrated after their trap-

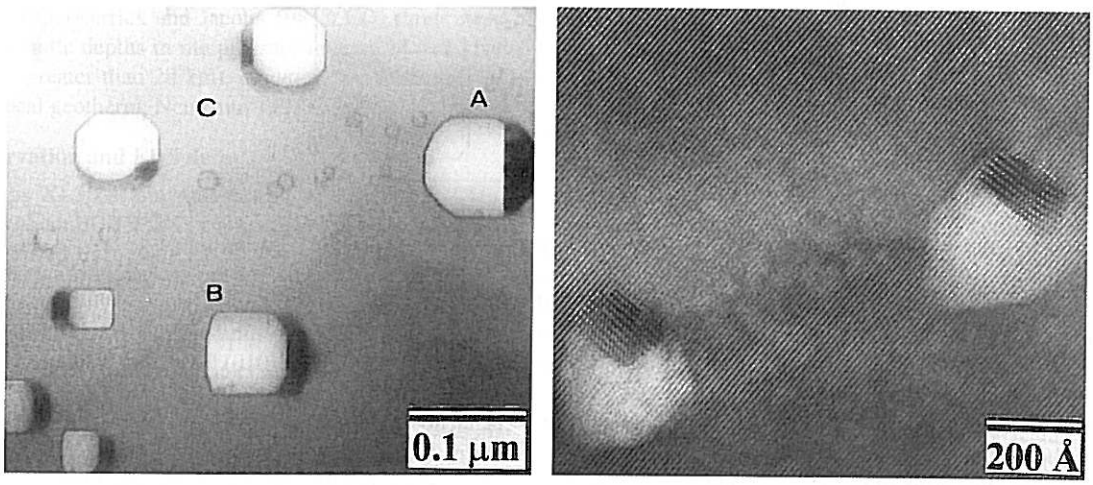

FIGURE 6. TEM images of olivine (**left**) Negative crystals with variable shape, size, and inner texture. Dark-faceted grains are evident within inclusion C. Tiny inclusions (~150–200 Å in diameter) are also present. (**right**) Crystalline grains within two inclusions: a Moiré pattern is produced due to the interference between lattice fringes of host olivine and daughter minerals. Sample TF14-48.

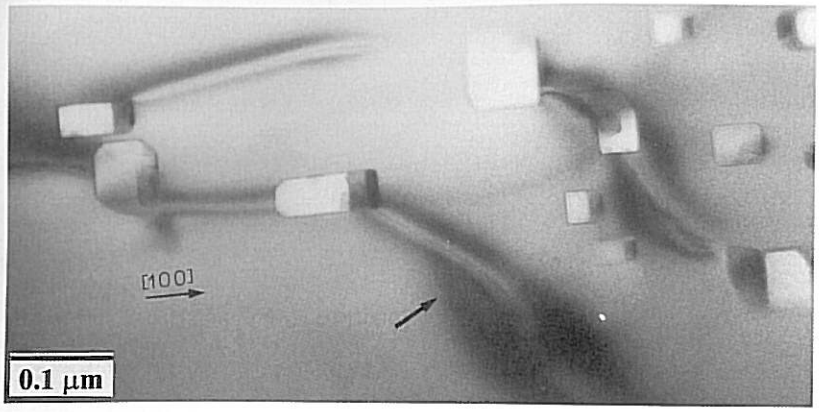

FIGURE 7. High-resolution TEM image showing sigmoidal contrast feature, shared by two to three different inclusions in a swarm-like trail and corresponding to healed microfractures. Note that healed microfractures are inclined with respect to both the main trail orientation (thick arrow) and the olivine [100] (thin arrow). Sample TF14-48.

ping. In the latter case, a knowledge of the mechanisms by which re-equilibration took place is of fundamental importance for the petrological interpretation of ThL data.

Only a few TEM studies of fluid inclusions have been done until now, possibly due to experimental difficulties. The first problem arises from TEM sample preparation. Samples have to be electron-transparent (that is, less than a few hundred angstroms thick): most inclusions are then disturbed during sample preparation, for instance by preferential ion milling and loss of the solid (glass or mineral) and by loss of the fluid. Another problem is the scale difference between TEM and optical microscopy: in fact, direct correlation between inclusions at the scale of the optical microscope and that of the transmission electron microscope is often difficult. Most TEM information is not obtained exactly from the same inclusions measured previously by optical microscopy. However, the main objective is to distinguish similar kinds of inclusions on the basis of their shape, composition, textural arrangement in trails (i.e., the basis for determining a common origin), independent of their absolute size. The principal findings of this study are discussed below.

Negative crystal morphology

Fluid ± glass inclusions <0.2 μm in diameter typically appear as negative crystals, whereas larger inclusions are essentially anhedral. Size has an important role in negative crystal evolution: the growth of perfect negative-crystal faces is energetically favored for small inclusions.

Negative crystals with different sizes, shapes, and inner textures may coexist in the same trail. The occurrence of negative crystals of variable size is not surprising: they probably result from the trapping of inclusions with different sizes, successively evolving to negative crystals. The size variability is related to the healing processes, in particular to the occurrence of minor microfractures associated with the main fracture (corresponding to the trail orientation): these healed microfractures are inclined with respect to the trail, indicating that healing took place both perpendicular to the main fracture and in oblique directions. The occurrence of different crystal habits is less obvious. In general, the shape of a crystal depends mostly on its structure and composition, together with the *P-T* conditions, growth rate, and degree of oversaturation. Negative crystals represent a peculiar situation: the shape is related to the structure of the host mineral (olivine), reasonably assumed to be constant. Similarly, the *P-T* conditions and the growth rate (here, the healing rate) should also be constant within the same trail. Therefore, we suggest that different habits arise from local chemical differences in the trapped material (i.e., from slightly different proportions among fluid phase, silicate, and sulfide melts). In particular, a fluid-rich inclusion (giving rise to a large, rounded bubble) could promote an equant growth of the (010) and (100) faces, whereas the trapping of fluid-poor, viscous silicate-melts could give rise to prismatic negative crystals.

CO_2 leakage through dislocations

At the TEM scale, fluid inclusions are commonly connected to dislocation arrays: these features, undetected at the scale of the optical microscope, are particularly abundant in sample TF14-48. This sample gave the highest values of ThL (i.e., lowest density values) as well as the greatest spread in density data, thus indicating that a re-equilibration process actually occurred. Re-equilibration may have occurred without partial decrepitation and/or stretching of fluid inclusions in shallow magma chambers: the mechanism of re-equilibration could be attributed to a CO_2-fluid leakage by pipe diffusion along dislocations.

The theoretical parameters that affect the efficacy of pipe diffusion include: (1) size of the molecule vs. size of the pipe and (2) adsorption and reactivity between molecules and the walls of the pipe. Unfortunately, very few experimental studies have been performed on two components (water and CO_2) or on CO_2 fluids, whereas most research on fluid diffusion deals with purely aqueous fluids. Belonoshko (1989) described the behavior of an aqueous-carbon dioxide fluid within thin pores, showing a preferential partitioning of CO_2 and H_2O in pores or in the fluid, as a function of variable pore size, variable fluid composition, and variable pressure and temperature. CO_2 molecules (0.5 up to 1.5 wt%) were identified within the open channels in the cordierite structure by Johannes and Schreyer (1981). These authors also performed high-pressure and high-temperature experiments, showing that the CO_2 content increases with *P* but decreases with *T*. Thus, CO_2 molecules may enter silicate structures and move by pipe diffusion, even if in lower amounts than water.

In the present study, we have indications that CO_2 molecules

have leaked from the inclusions and that they might have diffused along linking dislocations. The size of the stretched CO_2 molecule is 5.2–3.4 Å (length and width, respectively; Johannes and Schreyer 1981) and cell parameters of forsterite are 4.82, 10.48, 6.09 Å, with [100] and [001] as the most common Burgers vectors. CO_2 is an inert, non-polar molecule, and behaves differently from H_2O, in that it does not link to the pipe walls. Actually, a weak chemical affinity between CO_2 and olivine should not represent a hindrance for fluid leakage: in fact "partitioning of incompatible elements, for which there are no suitable crystallographic sites in normal rock-forming minerals, may be much more strongly influenced by dislocation densities than are compatible elements" (Buseck and Veblen 1978).

Petrological implications

Two different scenarios might be envisaged. Dislocations have formed at the end of healing processes, due to olivine crystal lattices misorientation: the fluid inclusion trails and the dislocation arrays mark the original fracture plane. Alternatively, it may be proposed that dislocations formed as the result of increased CO_2 pressure during cooling in the mantle or during ascent. Note that both processes do not require any deformation whatsoever of the host rocks.

The first scenario seems to be the most likely: in fact, if dislocations would have formed due to inclusion fluid overpressure, then all the fluid inclusions trapped in mantle olivine should show evidence for fluid loss, including samples from Hierro. The present study indicates that re-equilibration of fluid inclusions is particularly evident in the sample TF-14-48, which is also affected by intense deformation. Thus, it might be proposed that leakage by diffusion along dislocations would be enhanced by late deformation. Leakage would also be favored due to the strain caused by the inclusions' internal overpressure during the xenolith ascent.

It is evident that the low-density fluid inclusion data have no petrological significance and cannot be interpreted as due to the residence in magma chambers: extreme caution should be taken for the interpretation of density histograms, especially when the data distribution is very scattered.

Acknowledgments

Constructive reviwes by A.J. Brearley, W. Lamb, P. Raterron, and two anonymous referees have greatly improved the manuscript. The authors are indebted to E.-R. Neumann for useful discussions and for providing Hierro xenoliths. We further acknowledge T. Andersen and M. Mellini for critical reviews. G. Cavarretta is kindly acknowledged for providing to M.L.F. the microthermometry facilities at the C.S.Qu.E.A.–C.N.R in Rome. Raman microprobe facilities were provided by P.N.R.A., the Italian Organisation for Scientific Research in Antarctica.

References cited

Bakker, R.J. and Jansen, J.B.H. (1994) A mechanism for preferential H_2O leakage from fluid inclusions in quartz, based on TEM observations. Contributions to Mineralogy and Petrology, 116, 7–20.

Belonoshko, A.B. (1989) The thermodynamics of the aqueous carbon dioxide fluid within thin pores. Geochimica et Cosmochimica Acta, 53, 2581–2590.

Brown, P.E. (1989) FLINCOR a microcomputer program for the reduction and investigation of fluid inclusion data. American Mineralogist 74, 1390–1393.

Buseck, P.R. and Veblen, D.R. (1978) Trace elements, crystal defects and high resolution electron microscopy. Geochimica and Cosmochimica Acta, 42, 669–678.

Fleet, M.E. (1975) The growth habits of olivine–a structural interpretation. Canadian Mineralogist, 13, 293–297.

Frezzotti, M.-L., De Vivo, B., and Clocchiatti, R. (1991) Melt-mineral-fluid interactions in ultramafic nodules from alkaline lavas of Mount Etna (Sicily, Itally): melt and fluid inclusion evidence. Journal of Volcanological and Geothermal Research, 47, 209–219.

Frezzotti, M.-L., Burke, E.A.J., De Vivo, B., Stefanini, B., and Villa, I.M. (1992) Mantle fluids in pyroxenite nodules from Salt Lake Crater (Oahu, Hawaii). European Journal of Mineralogy, 4, 1137–1153.

Frezzotti, M.-L., Touret, J.L.R., Lustenhouwer, W., and Neumann, E.-R. (1994) Melt and fluid inclusions in dunite xenoliths from La Gomera, Canary Islands: Tracking the mantle metasomatic fluids. European Journal of Mineralogy, 6, 805–817.

Gurenko, A.A., Hansteen, T.H., and Schmincke, H.-U. (1996) Evolution of parental magmas of Miocene shield basalt, Gran Canaria, Canary Islands: constraints from crystal, melt and fluid inclusions in minerals. Contributions to Mineralogy and Petrology, 124, 422–435.

Hansteen, T.H., Andersen, T., Neumann, E-R., and Jelsma, H. (1991) Fluid and silicate glass inclusions in ultramafic and mafic xenoliths from Hierro, Canary Islands: implications for mantle metasomatism. Contributions to Mineralogy and Petrology, 107, 242–254.

Hansteen, T.H., Klugel, A., and Schmincke, H.-U. (1998) Multi-stage magma ascent beneath the Canary Islands: evidence from fluid inclusions. Contributions to Mineralogy and Petrology, 132, 48–65.

t'Hart, J.T. (1987a) The structural morphology of olivine. I—a qualitative derivation. Canadian Mineralogist, 16, 175–186.

———(1987b) The structural morphology of olivine. II—a quantitative derivation. Canadian Mineralogist, 16, 547–560.

Johannes, W. and Schreyer, W. (1981) Experimental introduction of CO_2 and H_2O into Mg-cordierite. American Journal of Science, 281, 299–317.

Kerrick, D.M. and Jackobs, G.K. (1981) A modified Redlich-Kwong equation for H_2O, CO_2 and H_2O-CO_2 mixtures at elevated temperatures and pressures. American Journal of Science, 281, 735–767.

Neumann, E.R. (1991) Ultramafic and mafic xenoliths from Hierro Canary Islands: evidence for melt infiltration in the upper mantle. Contributions to Mineralogy and Petrology, 106, 236–252.

Neumann, E.R., Wulff-Pedersen, E., Johnsen, K., Andersen, T., and Krogh, E. (1995) Petrogenesis of harzburgite and dunite suite xenoliths from Lanzarote, Canary Islands; implication for the upper mantle. Lithos, 35, 83–107.

Schiano, P. and Clocchiatti, R. (1994) World-wide occurrence of silica-rich melts in subcontinental and suboceanic mantle minerals. Nature, 368, 621–624.

Siena, F., Beccaluva, L., Coltorti, M., Marchesi, S., and Morra, V. (1991) Ridge to hotspot evolution of the Atlantic lithospheric mantle: evidence from Lanzarote peridotitic xenoliths (Canary Islands). Journal of Petrology, Special Lithosphere issue, 271–290.

Spera, F. (1984) Carbon dioxide in petrogenesis III: role of volatiles in ascent of alkaline magma with special reference to xenolith-bearing mafic lavas. Contributions to Mineralogy and Petrology, 88, 217–232.

Szabo, C.S. and Bodnar, R.J. (1996) Changing magma ascent rates in the Nograd-Gomor volcanic field Northern Hungary/Southern Slovakia: evidence from CO_2–rich fluid inclusions in metasomatised upper mantle xenoliths. Petrology, 4, 240–249.

Touret, J.L.R. (1992) CO_2 transfer between the upper mantle and the atmosphere: temporary storage in the lower continental crust. Terra Nova, 4, 87–98.

Veblen, D.R. (1985) Extended defects and vacancy non stoichiometry in rock-forming minerals. In R.N. Schock, Ed., Point Defects in Minerals, 3, 122–131. AGU Geophysical Monograph, 31, Washington, D.C., U.S.A.

Vityk, M.O. and Bodnar, R.J. (1995a) Do fluid inclusions in high-grade metamorphic terranes preserve peak metamorphic density during retrograde decompression? American Mineralogist, 80, 641–644.

———(1995b). Textural evolution of synthetic fluid inclusions in quartz during re-equilibration, with applications to tectonic reconstruction. Contributions to Mineralogy and Petrology, 121, 309–323.

Wanamaker, B.J. and Evans, B. (1989): Mechanical re-equilibration of fluid inclusions in San Carlos olivine by power-law creep. Contributions to Mineralogy and Petrology, 102, 102–111.

Wulff-Pedersen, E., Neumann, E.-R., and Jensen, B.B. (1996) The upper mantle under La Palma, Canary Islands: formation of Si-K-Na-rich melt and its importance as a metasomatic agent. Contributions to Mineralogy and Petrology, 125, 113–139.

Manuscript received August 23, 1999
Manuscript accepted June 2, 2000
Paper handled by Adrian J. Brearley